Journal of Drug Delivery Science and Technology 82 (2023) 104307

Contents lists available at ScienceDirect

Journal of Drug Delivery Science and Technology

journal homepage: www.elsevier.com/locate/jddst

Chitosan/agarose/graphene oxide nanohydrogel as drug delivery system of 5-fluorouracil in breast cancer therapy

Mariyeh Rajaei [a], Hamid Rashedi [a,**], Fatemeh Yazdian [b,***], Mona Navaei-Nigjeh [c], Abbas Rahdar [d,****], Ana M. Díez-Pascual [e,*]

[a] Department of Biotechnology, School of Chemical Engineering, Collage of Engineering, University of Tehran, Tehran, Iran
[b] Department of Life Science Engineering, Faculty of New Science and Technologies, University of Tehran, Tehran, Iran
[c] Pharmaceutical Sciences Research Center, The Institute of Pharmaceutical Sciences (TIPS), Tehran University of Medical Sciences, Tehran, Iran
[d] Department of Physics, Faculty of Sciences, University of Zabol, Zabol, 538-98615, Iran
[e] Universidad de Alcalá, Facultad de Ciencias, Departamento de Química Analítica, Química Física e Ingeniería Química, Ctra. Madrid-Barcelona, Km. 33.6, 28805, Alcalá de Henares, Madrid, Spain

ARTICLE INFO

Keywords:
Chitosan
Agarose
Drug delivery

ABSTRACT

Breast cancer refers to a very common deadly class of malignant tumors, especially in women worldwide. In the present study, a promising methodology has been developed to simultaneously improve the drug loading performance and achieve a sustained release of 5-fluorouracil (5-FU) as a model drug for breast cancer. For this purpose, a pH-sensitive and biocompatible hydrogel of chitosan/agarose/graphene oxide (CS/AG/GO) was first synthesized with glyoxal as cross-linker. 5-FU-loaded nanocomposites (NCs) of CS/AG/GO were then prepared via water-in-oil-in-water (W/O/W) emulsification technique. XRD and FTIR analyses confirmed the successful synthesis of the nanocarriers and gave insight on their crystalline structure and molecular interactions between the components. DLS demonstrated that the nanocarriers comprise nanoparticles with an average size of 197 nm and a PDI of 0.34. SEM revealed their spherical morphology and zeta potential measurements indicated an average surface charge of +23.5 mV. The drug loading and entrapment efficiencies (57% and 92%, respectively) were significantly higher than those reported previously for other nanocarriers. A very effective and sustained drug release profile was observed at pH 5.4; in 48 h, almost the entire 5-FU content was released. Moreover, effective cytotoxicity against breast cancer cell (BCC) lines (MCF-7) was observed: the cell viability upon incubation with CS/AG/GO/5-FU was about 23%, demonstrating its anti-cancer capability. Therefore, the synthesized NCs can potentially act as pH-sensitive nanovehicles for programmed release of 5-FU in breast cancer treatment.

1. Introduction

Caused by a common species of malignant tumors, breast cancer is a deadly disorder, especially in women, worldwide [1]. In the meantime, a better understanding of the tumor biology can contribute to effectiveness of treatment methods. In recent decades, application of new technology for understanding the cancers biologically and formulating effective treatments have developed dramatically [2]. Numerous approaches have been used to treat cancer, including chemotherapy, immunotherapy, radiotherapy, and surgery, and the combination of different strategies generally comes up with a more effective treatment [3]. Amongst them, chemotherapy is acknowledged as the most promising approach that can improve biocompatibility, bioavailability, effective targeting of the affected area, and safety of therapeutic drugs [4,5]. So far, various types of chemotherapeutic drugs have been investigated, and they show extensive side effects [6]. It is very important to protect non-engaged members and tissues of the body from potential poisoning before the chemotherapeutic drug is delivered to the

* Corresponding author.
** Corresponding author.
*** Corresponding author.
**** Corresponding author.
E-mail addresses: hrashedi@ut.ac.ir (H. Rashedi), yazdian@ut.ac.ir (F. Yazdian), mnavaei@sina.tums.ac.ir (M. Navaei-Nigjeh), a.rahdar@uoz.ac.ir (A. Rahdar), am.diez@uah.es (A.M. Díez-Pascual).

https://doi.org/10.1016/j.jddst.2023.104307
Received 19 November 2022; Received in revised form 20 February 2023; Accepted 23 February 2023
Available online 27 February 2023

tumor site [7]. Recently, much effort has been made to develop new approaches for the design of drug delivery systems [8]. An ideal drug carrier is the one that renders the insoluble anti-cancer drug into the tumor site and then releases the drug right at the target site with minimum side effects to the body [9]. Nanocarriers offer a good solution for targeted drug delivery, especially for water-insoluble drugs [10]. Amongst different nanocarriers (*e.g.*, liposomes [11], nanoparticles [12], nanogels [13], micelles [14], etc.), nanoparticles can exhibit more advantages due to their potential to ameliorate extant methods of cancer treatment.

Chemotherapy with 5-fluorouracil (5-FU) drug is the first line of complementary therapy for cancerous patients. 5-FU is a fluorinated pyrimidine that inhibits thymidine nucleotide biosynthesis by inhibiting the thymidylate synthase enzyme, which is supposed to end up with cell death [15]. It shows enhanced bioavailability, being applied as a strong drug against solid tumors. Considering that the use of 5-FU increases the patients' life expectancy, yet drug resistance has been reported in most cases, so that the effectiveness of 5-FU treatment has been reportedly as low as 26% [16]. Body resistance to an anticancer drug can cause different results, including a change in the drug penetration and flow, an increase in drug inactivation, and mutations in the drug target gene [17]. However, treatments are usually ineffective for advanced cancer. Accordingly, researchers are looking for other antitumor compounds to minimize the side effects of alternative cancer treatments [18].

Produced from natural or synthetic polymers, hydrogels can provide biocompatible, biodegradable, and non-toxic polymeric carriers. In this study, three compounds were used: chitosan (CS), agarose (AG), and graphene oxide (GO).

Graphene is an allotrope of carbon with a honeycomb structure [19]. Graphene and its derivatives such as graphene oxide (GO) have been synthesized via diverse methods, the most common approach being strong oxidation of graphite particles at a controlled temperature using the Hummer's method [20]. GO has been used in biomedical applications such as drug delivery, gene delivery, cancer diagnosis and treatment [21]. GO offers a very large specific surface area, high biocompatibility and hydrophilicity, and presents a diverse set of functional groups (*e.g.*, hydroxyl, carboxyl, and epoxy, among others) [22]. Due to its low dispersion in a physiological medium, GO is yet to be drug-loaded for effective drug delivery application. In this respect, different biologically active materials (*e.g.*, CS) have been used to ameliorate the dispersion of GO [23].

CS is a lineal cationic polysaccharide with prominent features such as low toxicity coupled with proper hydrophilicity, biocompatibility, biodegradability, low immunogenicity, constructional mutability, and participation in extended-release and drug permeation. These advantages made CS a natural biopolymer for hydrogels synthesis in drug delivery [24–26]. It is well known that CS responses to pH owing to the presence of amine groups. Due to these properties, CS has been frequently used as a biomedical substance and nanocarrier in drug delivery systems [27].

AG is an attractive lineal polysaccharide that exhibits crosslinking character during hydrogel formation for drug loading. Indeed, AG-containing hydrogels are very stable and biocompatible. Further, incorporation of AG into hydrogel structure creates some sort of pH-sensitivity [26,28]. To prepare an AG gel, heating and cooling operations are necessary. Thanks to its heat-reversible gel-making capability, AG has been used in various applications, including, but not limited to, DNA electrophoresis, tissue engineering, food industry, and drug delivery [29].

In this research, 5-FU was loaded onto a pH-sensitive hydrogel NC of CS/AG/GO for in vitro treatment of human BCC (MCF-7). To the best of our knowledge, no previous study dealing with such ternary hydrogel has been reported. This is the first biocompatible NC hydrogel made of two polysaccharides and GO that can potentially increase the dosage of 5-FU, as a model drug, through localization at the target site. Thus, the developed nanocarrier shows great potential for targeted release of 5-FU and effective breast cancer treatment.

2. Materials and methods

2.1. Materials

Table 1 lists the materials used in this research.

2.2. Synthesis of GO

GO was synthesized herein according to Hummer's method [30]. For this purpose, 1g of graphite sheets was introduced into 20 mL of H_2SO_4 solution while stirring the mix on a magnetic stirrer for 30 min. Next, 3 g of $KMnO_4$ was gradually added into the mix while the system was ice-cooled. Subsequently, 50 mL of distilled water was added dropwise and after 10 min, 100 mL of distilled water was poured into the mixture. After another 30 min, 35 mL of H_2O_2 was introduced into the solution, which turned to yellow/orange color. A homogeneous GO solution was obtained after 24 h. From this solution, powdery GO particles could be obtained by centrifugation followed by a dehydration stage in a vacuum oven.

2.3. Formation of CS/AG/GO hydrogel

As a first step, 20 mL of 2% v/v acetic acid was added dropwise to CS at 25 °C until a 20% w/v solution was achieved. Then, 1% w/v of AG was added to the CS solution and a CS/AG hydrogel was formed. Subsequently, 0.1% w/v GO was further added to the CS/AG hydrogel. All the steps were performed under vigorous stirring.

Table 1
General information on the materials used in this research.

Description (Code)	Manufacturer/ provider	City	Country
Human breast cancer cell (BCC) lines (MCF-7)	American Type Culture Collection (ATCC)	Manassas	VA, USA
Dulbecco's Modified Eagle's Medium (DMEM, high glucose)	Thermo Fischer Scientific	Waltham	MA, USA
Fetal bovine serum (FBS)	HyClone Thermo Scientific	Waltham	MA, USA
Penicillin-Streptomycin	Beijing Solarbio Science and Technology	Beijing	China
Trypsin (0.25% w/v) Ethylene-diamine-tetra-acetic-acid (EDTA, 0.1% w/v)			
3-(4, 5-dimethyl-thiazol-2-yl)-2,5-diphenyl-tetrazolium bromide (MTT)	Sigma-Aldrich	St. Louis	MS, USA
Dimethyl sulfoxide (DMSO)			
Chitosan (CS, Mw:50 kDa; DD:80–85%)			
Agarose (AG, gel strength >1200 gm/cm^2)			
Graphene oxide powder (GO, 15–20 sheets, 4–10% edge-oxidized)			
5-Fluorouracil (5-FU, Mw: 130.08 g/mol)			
Glyoxal (40 wt% in H_20)			
Polyvinyl alcohol (PVA; Mw:85000–124000; 99+% hydrolyzed)			
Phosphate buffer saline (PBS)	Iranian Biological Resource Center	Tehran	Iran
Span 80	Merck	Kenilworth	NJ, USA
Acetic acid			
Paraffin oil	CARLO ERBA Reagents	Comaredo	Italy

2.4. Drug loading and entrapment in the CS/AG/GO hydrogel

Taken as a model drug in this research, 2% (v/v) 5-FU was introduced into the prepared hydrogel solution in the previous step. This was carried out on a magnetic stirrer and the stirring was kept for 15 min to ensure complete mixing of the precursors. 0.02% v/v glyoxal was used as a crosslinker to form a homogenous 5-FU-loaded CS/AG/GO hydrogel. Finally, entrapment of 5-FU in the hydrogel structure was ensured as CS/AG were crosslinked to CS/AG/GO. Indeed, the crosslinking was obtained via reaction among the primary amines at the end of the polymer chains of CS and also between these free amines and the hydroxyl groups on GO and AG.

2.5. Preparation of double emulsion (DE)

Once the drug-loaded hydrogel NC was synthesized, the internal phase of a W/O/W DE was loaded with the NC to enhance its sustained-release behavior. For such purpose, an aqueous phase of hydrogel in oil was emulsified to obtain the base emulsion. Next, 5 mL of the drug-loaded hydrogel NC was introduced dropwise into a hydrophobic phase of paraffin oil (as dispersed phase; 60 mL) and 2% v/v Span 80 (as surfactant) under vigorous stirring. After 10 min, a hydrophilic phase of 1% v/v PVA (30 mL) was introduced dropwise into the base emulsion, and the mixture was stirred vigorously. Upon another 10 min, the stirring was stopped and the phases were separated by density. The hydrophobic phase, located on top of the hydrophilic phase, was removed. Then, a 5-min centrifugation stage (Hermle-Labnet) was applied at 4500 rpm to extract the DE from the remaining hydrophilic phase. The different steps to prepare the NC hydrogel and then encapsulating the NCs by the double nanoemulsion are schematically shown in Fig. 1.

2.6. Evaluating the efficiencies of drug loading and entrapment

The efficiencies of loading the model drug (5-FU) and then entrapping it in the CS/AG/GO hydrogel were assessed. For such purpose, lyophilized CS/AG/GO/5-FU hydrogel NCs were suspended in 1 mL of PBS before introducing 1 mL of ethyl acetate as organic solvent. The mixture was subjected to agitation, and the organic solvent was then removed. The amount of free 5-FU in the removed organic solvent was measured by means of UV–Vis spectrophotometry at 266 nm [31]. Equations (1) and (2) were used to estimate 5-FU encapsulation (EE) and loading (LE) efficiencies, respectively.

$$\text{Entrapment Efficiency}\,(\%)=\frac{(\text{Total amount of } 5-\text{FU})-(\text{Free amount of } 5-\text{FU})}{(\text{Total amount of } 5-\text{FU})}\times 100 \tag{1}$$

$$\text{Loading Efficiency}\,(\%)=\frac{(\text{Total amount of } 5-\text{FU})-(\text{Free amount of } 5-\text{FU})}{(\text{Total amount of Nanocomposite})}\times 100 \tag{2}$$

2.7. Characterization of the synthesized nanocarrier

To evaluate the surface morphology of the NCs, Field Emission Scanning Electron Microscopy (FESEM) was used at a voltage of 30 kV. The NCs average particle size distribution and surface charge were assessed by dynamic light scattering (DLS) analysis and zeta potential measurements on a Horiba SZ-100 Zeta Analyzer (Japan). Experiments were conducted at 90° scattering angle once the solution was probe-sonicated. Fourier transform infra-red (FTIR) spectra were acquired at ambient temperature, on lyophilized samples, in the wavenumber range of 600–4000 cm^{-1} using attenuated total reflection ATR technique with a FT-IR spectrophotometer (PerkinElmer Spectrum Version 10.03.06, UK). 1-mm thick KBr pellets were prepared by grounding 1 mg of each sample with KBr in a mortar. The crystalline structure of the samples was investigated by X-ray diffraction (XRD) analysis using a Brucker D2 Phaser diffractometer with CuKα1 radiation and a Ni filter. Diffractograms were recorded upon each stage of introducing a component to ensure that the model drug was properly complexed with the hydrogel. XRD data were analyzed with HighScore Plus software.

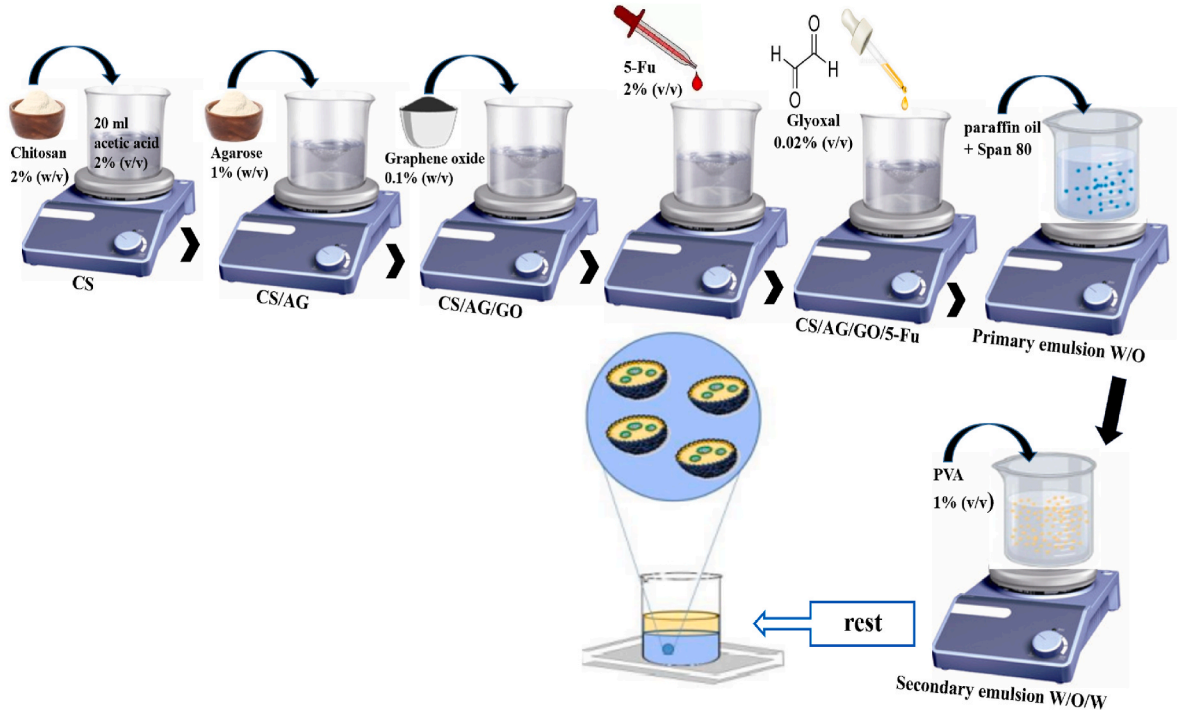

Fig. 1. Synthesis procedure for 5-FU-loaded CS/AG/GO NC hydrogel.

2.8. In vitro study of drug release

The release of 5-FU nanocarrier was investigated through the dialysis method [32] using two phosphate buffer media (pH 7.4 and 5.4) inside a water bath at 37 °C [33]. Firstly, 1 mL of CS/AG/GO/5-FU and CS/AG/GO were loaded into dialysis bags (Mw cut-off 12000 $gmol^{-1}$). Then, the bags were submerged in 50 mL of 20% v/v ethanol-bearing phosphate buffers. The ethanol increases the absorption and solubility of the drug, thereby accelerating its release. To assess how the DE affects the sustained release at pH 5.4, the amount of drug released from CS/AG/GO hydrogel into the DE was measured. At predefined periods of time (*i.e.*, 0, 12, 24, 48, 72, and 96 h), 300 μL of the tested sample was removed and substituted by the same volume of fresh 20% v/v ethanol-containing PBS. The released drug content in the buffer was assessed by UV–Vis spectrophotometry at a wavelength of 266 nm (U.V-T60U; PG Instrument, England) [34,35]. All the experiments were performed in triplicate and the percentage of drug release was calculated using Equation (3):

$$\text{drug released}\ (\%) = \frac{[5-\text{FU}]\text{rel}}{[5-\text{FU}]\text{load}} \times 100 \quad (3)$$

where $[5\text{-FU}]_{load}$ and $[5\text{-FU}]_{rel}$ are the loaded and then released amounts of 5-FU onto and from the NCs, respectively. To confirm the pH-responsive release behavior of the developed platform, the statistical analysis ANOVA was performed by comparing the release percentage of 5-FU from CS/AG/GO at pH 5.4 with all other groups.

2.9. Cell culture

The BCC (MCF-7) was cultured in DMEM upon supplementing with 10% FBS, 100 U/mL Penicillin, and 100 μg/mL Streptomycin at 37 °C inside a humidified incubator that was previously loaded with 5% CO_2.

2.10. Cytotoxicity assessment

Free 5-FU, 5-FU-loaded CS/AG/GO hydrogel NCs, and drug-free CS/AG/GO hydrogel NCs were subjected to cytotoxicity evaluation against MCF-7 using MTT assay. The cells were grown into a tissue culture incubator at 37 °C in presence of 5% CO_2. Each well of a 96-well plate was loaded with the appropriate amount of the growth medium (including 2×10^4 cells) and the plate was subjected to overnight incubation to ensure cell attachment. Upon achieving 70%-confluent cells, cell treatment was performed with the considered samples at a dosage of 5 μg/mL (*i.e.*, concentration of 5-FU in the nanocarrier carrying the drug-loaded CS/AG/GO hydrogel after correcting for the loading efficiency of the drug). The comparison between different samples at the same concentration enables to assess the impact of the fabricated nanocarrier on cytotoxicity, as is represented by variations in the release mode. 5-FU-free control cells were also grown in DMEM with FBS (10%) and penicillin-streptomycin (1%) as the base medium while keeping the same culturing time. After 72 h, the supernatant was removed, and 50 μL of fresh DMEM as well as 50 μL of MTT (5 mg/mL) were introduced in each well before an incubation stage of 3–4 h. Subsequently, each well was loaded with 150 μL of DMSO and simultaneously was shaken to ensure the dissolution of the formazan crystals. An ELISA multi-well scanning spectrophotometer operating at 570 nm was used to evaluate the optical density. All the experiments were performed in triplicate. The viability of the different groups was expressed as a percentage of the control, taking 100% viability for the control. For each treatment, the cell viability was estimated as mean ± standard deviation. The statistical analysis between groups was accomplished by GraphPad InStat 3 software by comparing the number of replicates (N = 3) in each group, the mean and the standard error of the mean.

2.11. Cell apoptosis assay

Apoptosis and necrosis analyses were carried out after Annexin V-FITC/Propidium Iodide (PI) coloring. Firstly, MCF-7 cells were treated with the free drug, drug-loaded CS/AG/GO hydrogel, and drug-free CS/AG/GO for 72 h. Cells were treated with the samples at a concentration of 5 μg/mL, as explained previously. After the treatment, the cells were removed, washed with cold PBS, and suspended within 500 μL of the binding buffer before coloring. Subsequently, they were incubated for 15 min under dark conditions and the result was assessed by a flow cytometer. The cells were then subjected to fluorescence intensity scanning within FL-1 (FITC) and FL-3 (PI) channels. Quadrant statistics were evaluated for the cell portions falling in various quadrants. According to the results, each panel refer to percent of Q1 (necrotic), Q2 (late apoptotic), Q3 (early apoptotic), and Q4 (viable cells). Noteworthy, all tests were conducted in triplicate to check for the improvement of apoptosis by sustained-release of 5-FU out of the drug-loaded CS/AG/GO/NCs.

3. Results

3.1. FTIR spectroscopy

FTIR spectra were acquired to corroborate the presence of all the components in the hydrogel NCs by analyzing their characteristic absorption peaks, as well as to get insight about the interactions between CS, AG, GO, and 5-FU. Besides, they proved the successful synthesis of GO.

In the FTIR spectrum of CS (Fig. 2a), the out-of-plane CH bending of monosaccharide rings corresponds to the peak at 890 cm^{-1}. A wide peak was observed within 2990–3580 cm^{-1}, which is related to N–H and O–H stretching vibrations, and the shape indicates hydrogen bonding between the molecules. The absorption band centered at 2854 cm^{-1} is ascribed to C–H stretching vibrations, in agreement with the observations reported for other polysaccharides [36–38]. The peaks at 1590 cm^{-1} and 1372 cm^{-1} can be attributed to the stretching of C═O and C–N bonds of amide I and amide III, respectively. The N–H bending of primary amines corresponds to the band at 1585 cm^{-1} [39]. The C–O stretching appears at 1060 and 1020 cm^{-1}. Finally, the absorption bands at 1416 and 1372 cm^{-1} are related to CH_2 bending and symmetrical CH_3 deformation, respectively [40].

In the spectrum of CS/AG (Fig. 2b), the characteristic C–H bending at 890 cm^{-1} was also observed. The C–O stretching was found herein at 1024 cm^{-1}, with a slightly decreased intensity and a small shift

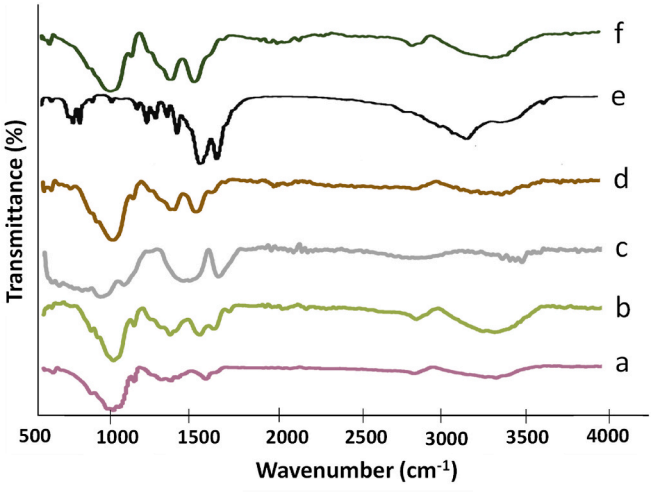

Fig. 2. FTIR spectrum of CS (a), CS/AG (b), GO (c), CS/AG/GO (d), 5-FU (e), and CS/AG/GO/5-FU(f).

compared to neat CS due to the introduction of AG. The shift in the characteristic amide group of CS from 1585 to 1551 cm^{-1} was also a result of the presence of AG, that increased the hydrogen bonding between molecules [41,42]. The peak at 2867 cm^{-1} was ascribed to C–H stretching vibrations of CH_2 of both AG and CS. O–H stretching was identified by a peak at 3343 cm^{-1}, showing decreased intensity compared to neat CS, likely due to molecular interactions between the hydroxyl groups of both polymers.

The FTIR spectrum of neat GO (Fig. 2c) shows characteristic peaks at 3390, 1698, and 1448 cm^{-1}, related to the stretching vibrations of O–H, C═O, and C–O functional groups, respectively. The C═O bond on the alkoxy group of GO was characterized by the peak at 1084 cm^{-1} [43].

In the FTIR data of CS/AG/GO NC (Fig. 2d), the absorption peak at 1149 cm^{-1} was found to be related to C–O stretching vibrations, indicating the presence of the epoxy group [44]. In addition to the characteristic peaks of AG and CS, a new peak emerged at 1621 cm^{-1} attributed to the amide I band, suggesting the formation of amide bonds between the carboxyl (COOH) groups in GO and amine groups (NH_2) in CS [45]. Stretching vibrations of C–O or C–O–C bonds of epoxy and alkoxy groups were observed at 1032 cm^{-1} [46]. These results confirmed the formation and chemical composition of CS/AG/GO NC.

The neat drug (Fig. 2e) exhibits peaks at 3200, 1710, 1630 and 1400 cm^{-1} due to the secondary amino (N–H) stretching, cyclic ketonic group, the C═C stretching, and C–F group, respectively. In the spectrum of the 5-FU-loaded hydrogel (CS/AG/GO/5-FU, Fig. 2f), peaks at 648, 1395, and 1531 cm^{-1} were found, which could be associated with C–H, C–N, and N–H bending vibrations, respectively. The peaks of the neat drug were also observed, which corroborate the presence of 5-FU in the NC. However, the peaks were shifted compared to the free drug. In particular, the shift in the position of the bands in the range of 3100–3600 cm^{-1} and 1700-1500 cm^{-1}, as well as the disappearance of the band at 1710 cm^{-1} further confirmed the formation of drug-NC hydrogen bonds between the amide groups in the nanocomposite and oxygen and fluorine atoms in the drug structure [47,48].

3.2. XRD analysis

XRD data was employed to monitor the changes in the crystalline structure upon introducing each component in the composite. The XRD pattern of neat CS shows a sharp diffraction peak at $2\theta = 20.4°$, related to amine II "–NH_2" of chitosan, in agreement with previous reports [49]; however, not peak at around 10°–11° related to amine I "–N–CO–CH_3" of chitosan was found, indicating a low level of crystallinity. In fact, CS has been reported to have semi-crystalline nature, with a level of crystallinity dependent on a number of parameters such as the DD and Mw [49]. In the diffractogram of CS/AG, the peak at $2\theta = 20.3°$ became broader, indicative of the amorphous nature of the mixture, since AG polymer is amorphous [50]. The XRD pattern of GO in Fig. 3c shows its amorphous structure, with a dominant peak at $2\theta = 23.6°$, indicating high interlayer distance [51]. Its structure is dependent on the type of synthesis and oxidation degree. In the XRD pattern of CS/AG/GO (Fig. 3d), a broad peak can be found in the range of $2\theta = 18–27°$ due to the amorphous nature of the NC. According to literature, 5-FU exhibits a crystalline structure with characteristic peaks in the 2θ range of 16-33°. Regarding CS/AG/GO/5-FU NC hydrogel (Fig. 3e), a broad amorphous profile is observed with some overlapped small crystalline peaks in the range of 17-33°, thus corroborating the successful encapsulation of 5-FU by carrier and proper dispersion of the drug within CS/AG/GO NCs [52,53].

3.3. Morphological studies

The surface morphology of 5-FU-loaded freeze-dried hydrogel NCs was studied via FESEM analysis (Fig. 4). Microscopic images at different magnifications clearly indicate that most of the NCs exhibit a uniformly spherical structure, which is the most desirable form of nanoparticles for drug delivery applications [54], with sizes in the range of 50–200 nm. The NC was well compatible with the drug, as clearly shown by its homogeneous surface.

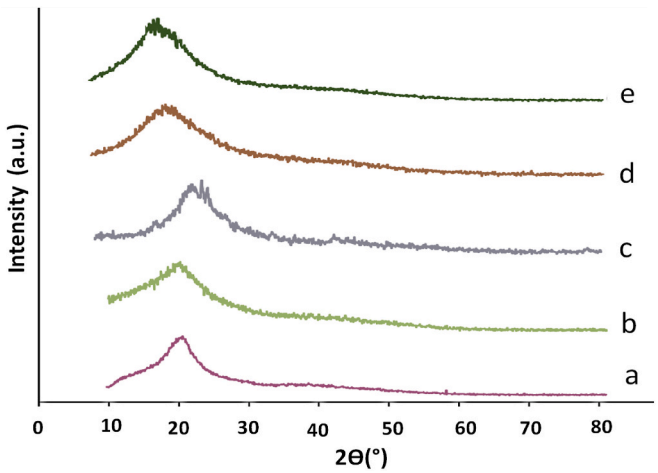

Fig. 3. XRD spectrum of CS (a), CS/AG (b), GO (c), CS/AG/GO (d), and CS/AG/GO/5-FU (e).

DLS data were analyzed to get information about the nanocarrier in terms of size and polydispersity. According to the results, the nanocarrier was found to be made up of particles with a PDI index of 0.34, and sizes in the range of 160–350 nm (Fig. 5), with an average value of 197 nm. According to the literature, this is an acceptable value of polydispersity for drug delivery systems [55]. The differences in size obtained via SEM and DLS are likely related to the fact that nanoparticles were dried prior to SEM observation, which is performed in the solid state, while DLS is carried out in solution and gives the hydrodynamic diameter, that takes into account the hydration layer, and is influenced by many factors including the surface charge, density, exposed surface ligands, the nature of the solvent, etc. Similar observations have been previously reported for other hydrogels designed for drug delivery [56,57].

Zeta potential measurements on the nanocarriers showed a mean value of +23.5 mV (Fig. 6); this high value confirms the good stability of the nanocarrier [56]. It is worthy to note that zeta potential values are high despite the use of PVA, a non-ionic surfactant, for the preparation of the nanocarrier. This can be explained considering that zeta potential depends on various parameters including particle size and dispersion environment (type of solvent, polar or non-polar). However, the effect of the particle size is stronger than the dispersion medium. Therefore, even though PVA decreases the zeta potential, the effect of nanocarrier particle size predominates, and the overall effect is an increase in zeta potential. This is an important parameter to maintain the overall integrity of the NC.

3.4. Drug loading and entrapping efficiency

After measuring the free 5-FU content of the ethyl acetate phase via UV–Vis spectrophotometry at 266 nm, the drug loading (LE) and entrapment (EE) efficiencies were estimated to be 92 and 57%, respectively. Indeed, these efficiencies are very high compared to those of other nanocarriers used in former studies, as shown in Table 2. The desirable drug loading efficiency was largely due to the porous nature of the nanoparticles, boosting the capacity of the nanoparticles for entrapping more drug molecules. In a former research, depending on 5-FU dosage, LE and EE were reported in the ranges of 1.6–52.5% and 16.4–66.5%, respectively, when lightweight dual sensitive core-shell hybrid nanospheres were utilized as an intelligent carrier for different pH and photothermal conditions [57]. Other researchers reported EE and LE of 84.7 and 37.2, respectively, when 5-FU was employed as

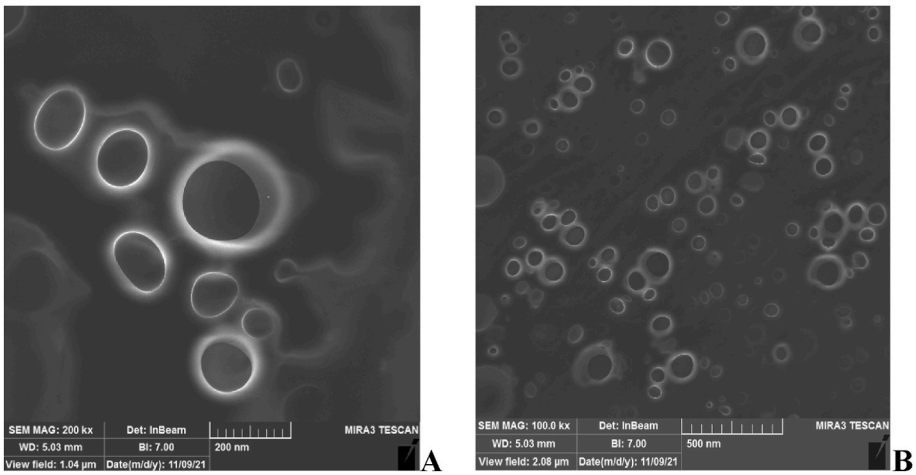

Fig. 4. FESEM images of CS/AG/GO/5-FU. A and B show images with scale bar of 200 and 500 nm, respectively.

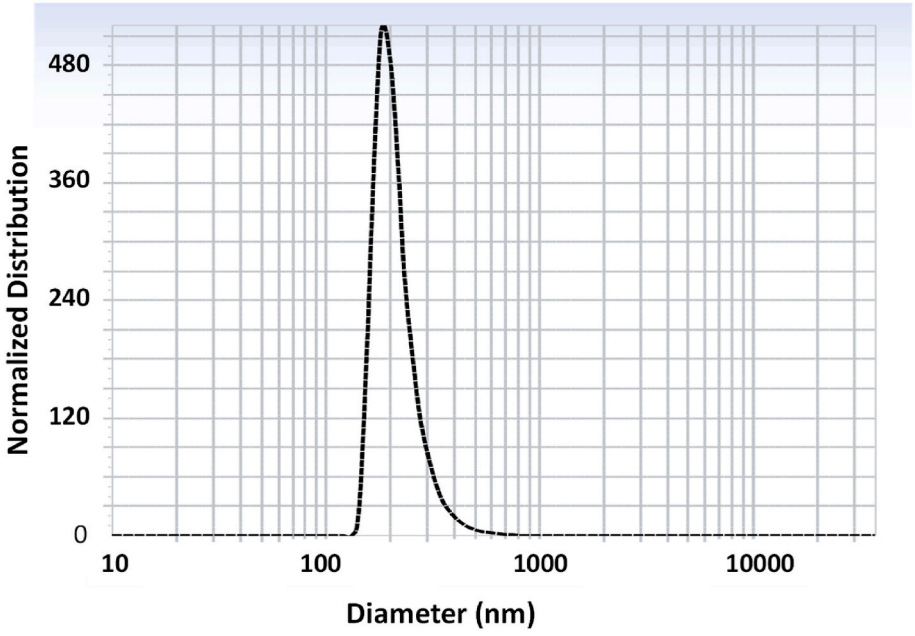

Fig. 5. Size distribution of the synthesized NC obtained by DLS.

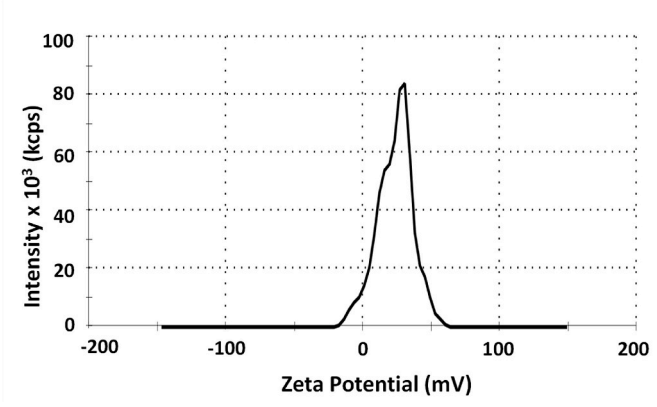

Fig. 6. Zeta potential of the synthesized NC.

Table 2
Comparison of entrapment efficiency (EE%) for different 5-FU nanocarriers.

Drug carrier	EE%	Reference
Core-shell hybrid nanospheres	16.4–66.5	[58]
Mesoporous silica nanoparticles	18.02	[59]
CS gold composite	41	[60]
CS nanoparticle	7.7–20.9	[61]
CS/AG/GO	92	This work

sample drug in CS/carbon quantum dot/aptamer NC [27].

The mechanism of drug loading is likely chemical adsorption. For drugs with low molecular weight, such as 5-FU, chemical interactions predominate. The type and strength of the chemical interaction is essential for the stability of the drug-loaded nanocomposite to prevent drug leakage from the nanocomposite channel. The strong hydrogen bonding interactions between the amide groups formed in the nanocomposite and oxygen and fluorine atoms in the drug structure as well as between NH bonds in the drug and hydroxyl groups in the nanocomposite, as inferred from the FTIR spectra, are believed to be

responsible for the high drug loading.

3.5. Drug release

The purpose of evaluating the release behavior of the nanocarrier was to ensure its pH-sensitivity and its capability for providing sustained drug release. Accordingly, the release of drug from the hydrogel NC was investigated by the methodology explained in Section 2.8, and the percentages of drug released as a function of time are shown in Fig. 7. As can be observed, the drug-loaded CS/AG/GO NC at pH 7.4 gradually released 29% of its 5-FU content in 24 h (Table 3). The presence of PVA as a surfactant in the aqueous phase of the secondary emulsion further stabilizes the nanocarrier and prolongs the release period [62]. The release rate was however much higher at pH 5.4 (acidic medium), in which the drug-loaded NC released about 65% of its 5-FU content in 24 h. This finding corroborates the pH-sensitivity of the synthesized nanocarrier. In 48 h, almost the entire 5-FU content of the drug-loaded NC was released at pH 5.4, while about half of the drug was still non-released from the NC when the pH was set to 7.4.

The observed trend may be due to the characteristic feature of CS biopolymer that leads to the opening of the pores and 5-FU release in acidic pH. However, at higher pH, the collapse of the CS chains leads to a reduction in the 5-FU release. The electrostatic repulsion between the protonated free amino groups on CS and 5-FU at pH 5.4 could be another explanation for the higher 5-FU release in acid medium. On the other hand, GO comprises carboxyl, hydroxyl, ketone and ether groups, that enable to interact with polar polymers like CS and AG. The mechanism of action of the nanocomposite is likely based on the formation of amide bonds between the carboxyl (COOH) groups in GO and amine groups (NH_2) in CS, as well as on some imine bonds between the ketone groups of GO and amine groups of CS. These bonds can be quickly cleaved in the intracellular acidic condition and lead to the release of the entrapped 5-FU [63]. Besides, H-bonds are formed between the hydroxyl, amine and amide groups in the nanocomposite and the functional groups of 5-FU (N–H, C–F, C═O), as confirmed by FTIR analysis. In an acidic media, protons can attack rich-electron site of the 5FU molecule, and the C = O bond is the most preferred [64], thus weakening the H-bonds, and in turn leading to a faster release.

Overall, the proposed NC shows a sustained and pH-sensitive drug release behavior that tends to improve targeted drug release for treating malignant tumor tissues, thereby alleviating possible side effects of the drug on normal cells [31].

Table 3
Comparison of drug release data at pH = 5.4 and pH = 7.5.

Time (h)	Release (%) (pH = 5.4)	Release (%) (pH = 7.4)
0	0	0
12	34.2 ± 1.5	11.3 ± 1.0
24	64.8 ± 3.6	29.1 ± 1.2
48	81.9 ± 2.8	56.3 ± 4.2
72	90.8 ± 2.1	66.9 ± 3.7
96	96.0 ± 2.9	78.9 ± 2.3

3.6. Cytotoxicity study

Fig. 8 shows the results of the cytotoxicity study of CS/AG, CS/AG/GO, drug-loaded CS/AG/GO and free 5-FU against BCC (MCF-7) via MTT assay after a 72 h incubation stage. Cell viability of the different systems was also evaluated against a control group (not treated). According to Fig. 8, about 68% and 78% cell viability is found for CS/AG/GO and CS/AG, respectively. The lower viability of MCF-7 cells upon exposure to CS/AG/GO NC rather than CS/AG confirmed the in vitro cytotoxicity of GO.

The cell proliferation was considerably reduced when they were treated with free 5-FU ($p < 0.001$). Moreover, encapsulation of 5-FU in CS/AG/GO reduced the cell viability significantly ($p < 0.001$). Thus, 5-FU-loaded CS/AG/GO was more cytotoxic than free 5-FU ($p<0.05$), possibly due to the steady drug release from the nanostructures over a long period of time.

The cell viability of CS/AG/GO/5-FU was estimated to be 23%, which indicates its considerable toxicity to cancer cells. Though the cell viability of CS/AG/GO/5-FU was almost identical to that of the free drug, it should be noticed that the released amount of drug at any particular point in time is smaller with the NC system rather than the free 5-FU because of the gradual drug release from the nanocarrier. Our findings demonstrate the high cytocompatibility of the drug-loaded CS/AG/GO hydrogel system as a drug delivery platform for anti-cancer drugs.

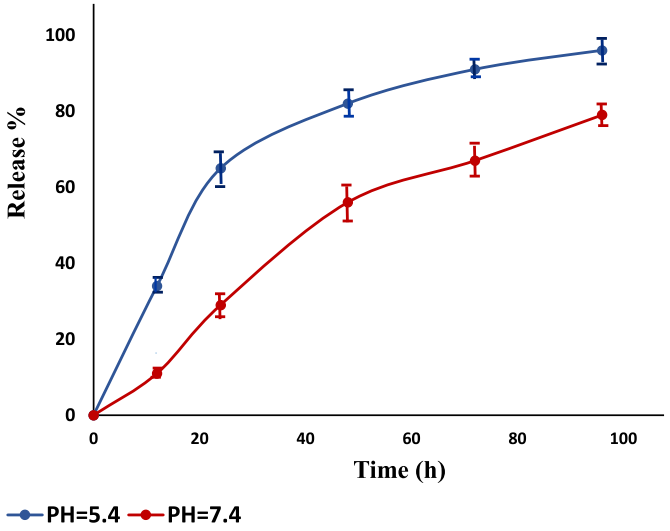

Fig. 7. Percentage of release of 5-FU from the NC hydrogel as a function of time. Measurements were carried out in triplicate at two different pH using dialysis method. Statistical analysis carried out between groups displayed significant difference between pH 5.4 with control group and all other groups with $p < 0.001$.

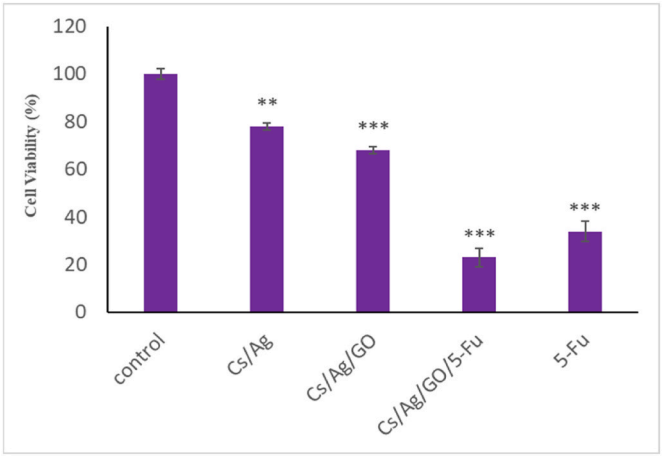

Fig. 8. Cell viability percentage of treated BCC (MCF-7). All the experiments were performed in triplicate and relative to the control group that had 100%. Discrepancy between control, free 5-FU, and 5-FU loaded in CS/AG/GO is considerable at $p < 0.001$. Discrepancy between free 5-FU and 5-FU loaded in CS/AG/GO is considerable at $p < 0.05$. [*** represents p-value ≤0.001 compared to control].

3.7. Cell apoptosis assay

Flow cytometry-based apoptosis analysis was carried out by an annexin V-FITC/PI apoptosis diagnosis kit to estimate the percentage of cells engaged with apoptosis and necrosis under the effect of CS/AG, CS/AG/GO, 5-FU-loaded CS/AG/GO, and free 5-FU (Fig. 9). Different quadrants are indicated on the flow cytometry diagram, where necrotic (FITC–/PI+), late apoptotic (FITC+/PI+), early apoptotic (FITC+/PI–),

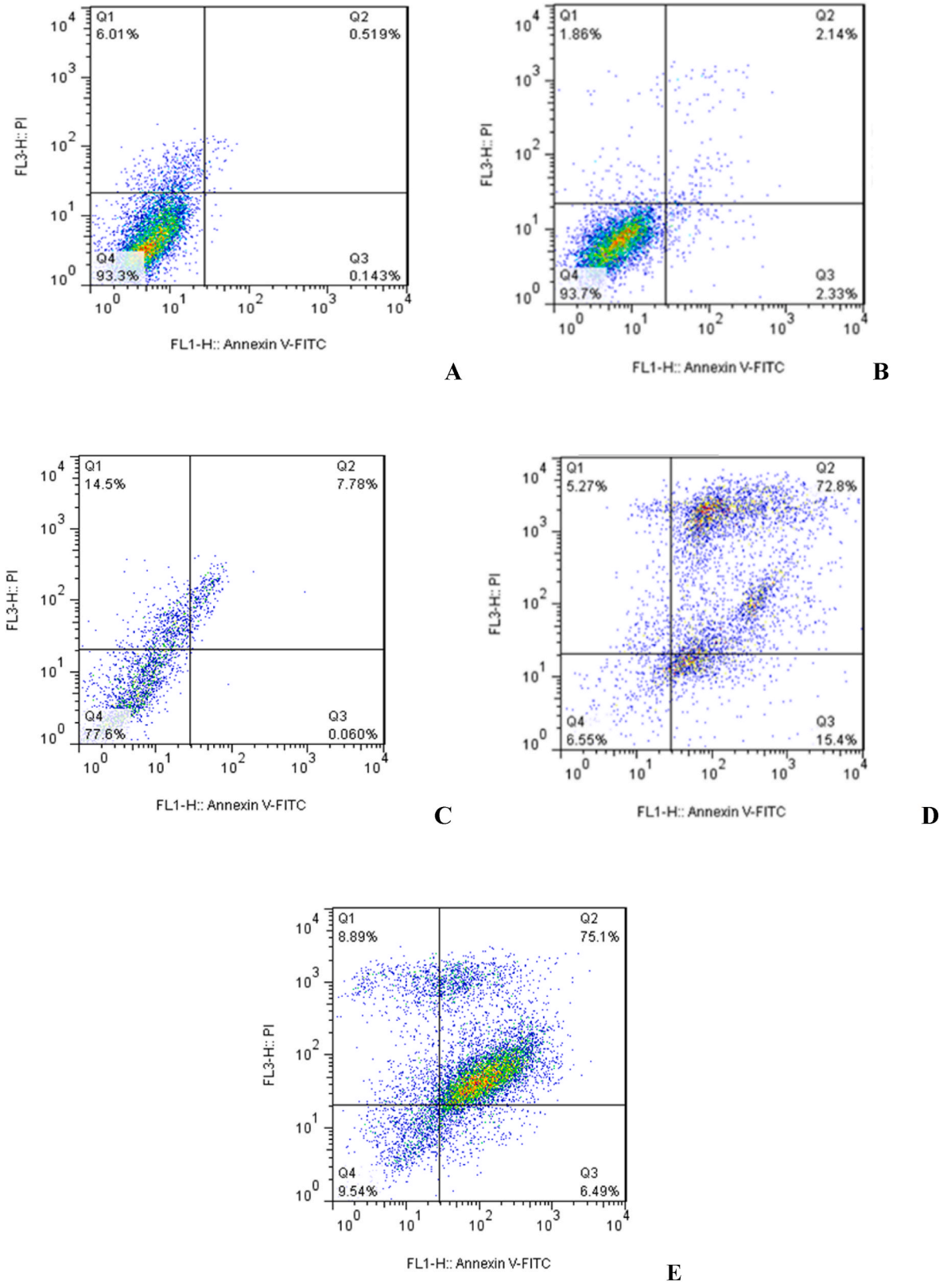

Fig. 9. Apoptotic analyses via flow cytometry of MCF-7 BCC treated for 72 h. A, B, C, D, and E indicate control, CS/AG, CA/AG/GO, CS/AG/GO/5-FU, and free 5-FU, respectively.

and alive cells (FITC–/PI–) fall within Q1 through Q4, respectively. Also, considering the percentages of live cells in CS/AG and CS/AG/GO nanocomposites, no significant differences with the control group are observed, which indicates biocompatibility and non-toxic characteristics of the free nanosystems. As shown in Figs. 9 and 0.143% and 0.519% of the cells were engaged with apoptosis in the early and late apoptotic phases, respectively, reflecting natural viability for the control cells. Conversely, 81.59%, 8.38%, and 88.2% of the cells ended up being engaged with the apoptosis upon treatment by free drug, pure CS/AG/GO, and drug-loaded CS/AG/GO NCs, respectively. These findings suggest that pure CS/AG/GO and drug-loaded CS/AG/GO NCs can significantly suppress the MCF-7 cells survival rate – a finding that is in agreement with the results of Section 3.4.

4. Conclusions

In this study, CS/AG/GO/5-FU nanocomposite hydrogel was successfully synthesized via W/O/W emulsification technique. The composition and interaction between the nanocarrier components and its crystalline structure were confirmed by FTIR and XRD analyses. The nanocarrier showed a spherical morphology, with an average size of 197 nm and a PDI of 0.34, as revealed by SEM and DLS techniques, respectively. Besides, its average surface charge was +23.5 mV, which confirms its good stability. The drug loading and entrapment efficiencies were 57% and 92%, respectively, significantly higher than those reported in former studies. A sustained drug release profile was observed in an acid medium, in which almost 100% drug released in 2 days. Also, the cell viability against breast cancer cell (BCC) lines (MCF-7) was around 23%. Encapsulation of 5-FU drug within the nanocarrier was found to improve the sustained drug release profile and pH-sensitivity, as well as the anti-cancer performance of the proposed drug delivery system. Our findings indicate that the formulated nanocarrier has high potential for pH-selective release of 5-FU (as a model drug) in a controlled manner for breast cancer treatment. Nonetheless, additional research is needed prior to its use in clinical trials. Thus, future work will investigate its cytotoxicity against healthy cells using human fibroblasts.

Funding

Financial support from the Community of Madrid within the framework of the multi-year agreement with the University of Alcalá in the line of action “Stimulus to Excellence for Permanent University Professors”, Ref. EPU-INV/2020/012, is gratefully acknowledged.

Author statement

Mariyeh Rajaei, Mona Navaei-Nigjeh: Writing—original draft (doing all experiments and invitro studies, and other studies and then results, and physico-chemical charaterization analysis). Hamid Rashedi, Fatemeh Yazdian: Conceptualization. Abbas Rahdar, Fatemeh Yazdian, Ana M. Díez-Pascual: Writing – review & editing. Fatemeh Yazdian, Hamid Rashedi: Supervision.

Declaration of competing interest

The authors declare that they have no known competing financial interests or personal relationships that could have appeared to influence the work reported in this paper.

Data availability

Data will be made available on request.

References

[1] Mitra Dolatkhah, et al., Graphene-based multifunctional nanosystems for simultaneous detection and treatment of breast cancer, Colloids Surf. B Biointerfaces 193 (2020), 111104.
[2] Kandasamy Vinothini, et al., Folate receptor targeted delivery of paclitaxel to breast cancer cells via folic acid conjugated graphene oxide grafted methyl acrylate nanocarrier, Biomed. Pharmacother. 110 (2019) 906–917.
[3] Cancer Facts & Figures 2019, American Cancer Society, Atlanta, USA, 2019, pp. 29–71.
[4] W. Jiang, H. Zhang, J. Wu, G. Zhai, Z. Li, Y. Luan, S. Garg, CuS@MOF-based welldesigned quercetin delivery system for chemo–photothermal therapy, ACS Appl. Mater. Interfaces 10 (2018) 34513–34523.
[5] D. Zhang, J. Zhang, Q. Li, H. Tian, N. Zhang, Z. Li, Y. Luan, pH- and enzymesensitive IR820–paclitaxel conjugate self-assembled nanovehicles for near-infrared fluorescence imaging-guided chemo–photothermal therapy, ACS Appl. Mater. Interfaces 10 (2018) 30092–30102.
[6] Malihe Pooresmaeil, Elnaz Aghazadeh Asl, Namazi Hassan, A new pH-sensitive CS/Zn-MOF@ GO ternary hybrid compound as a biofriendly and implantable platform for prolonged 5-Fluorouracil delivery to human breast cancer cells, J. Alloys Compd. 885 (2021), 160992.
[7] R. Cheng, R. Zou, S. Ou, R. Guo, R. Yan, H. Shi, S. Yu, X. Li, Y. Bu, M. Lin, Graphene oxide complex as a pH-sensitive antitumor drug, Polym. Chem. 6 (13) (2015) 2401–2406.
[8] S. Javanbakht, A. Shaabani, Encapsulation of graphene quantum dot-crosslinked chitosan by carboxymethylcellulose hydrogel beads as a pH-responsive bionanocomposite for the oral delivery agent, Int. J. Biol. Macromol. 123 (2019) 389–397.
[9] Y. Wang, M.S. Shim, N.S. Levinson, H.W. Sung, Y. Xia, Stimuli-responsive materials for controlled release of theranostic agents, Adv. Funct. Mater. 24 (2014) 4206–4220.
[10] H. Maeda, T. Sawa, T. Konno, Mechanism of tumor-targeted delivery of macromolecular drugs, including the EPR effect in solid tumor and clinical overview of the prototype polymeric drug SMANCS, J. Contr. Release 74 (1–3) (2001) 47.
[11] A.N. Cadinoiu, D.M. Rata, I.A. Leonard, O.M. Daraba, D. Gherghel, G. Vochita, M. Popa, Aptamer-functionalized liposomes as a potential treatment for basal cell carcinoma, Polymers 11 (9) (2019) 1515.
[12] Nasrin Zohreh, Nafiseh Karimi, Seyed Hassan Hosseini, Cosmin Istrate, Cristina Busuioc, Fabrication of a magnetic nanocarrier for doxorubicin delivery based on hyperbranched polyglycerol and carboxymethyl cellulose: an investigation on the effect of borax cross-linker on pH-sensitivity, Int. J. Biol. Macromol. (2022), 0141-8130.
[13] Rata Delia Mihaela, Anca Niculina Cadinoiu, Leonard Ionut Atanase, Marcel Popa, Cosmin-Teodor Mihai, Carmen Solcan, Lacramioara Ochiuz, Gabriela Vochita, Topical formulations containing aptamer-functionalized nanocapsules loaded with 5-fluorouracil-An innovative concept for the skin cancer therapy, Mater. Sci. Eng. C 119 (2021), 111591.
[14] Ketan Kuperkar, Dhruvi Patel, Leonard Ionut Atanase, Pratap Bahadur, Amphiphilic block copolymers: their structures, and self-assembly to polymeric micelles and polymersomes as drug delivery vehicles, Polymers 14 (21) (2022) 4702.
[15] Iurciuc Tincu, Camelia Elena, Monica Stamate Cretan, Violeta Purcar, Marcel Popa, Oana Maria Daraba, Leonard Ionut Atanase, Lacramioara Ochiuz, Drug delivery system based on pH-sensitive biocompatible poly (2-vinyl pyridine)-b-poly (ethylene oxide) nanomicelles loaded with curcumin and 5-fluorouracil, Polymers 12 (7) (2020) 1450.
[16] J. Wils, P. O'Dwyer, R. Labianca, Adjuvant treatment of colorectal cancer at the turn of the century: European and US perspectives, Ann. Oncol. 12 (1) (2001) 13–22.
[17] E. Eftekhar, F. Naghibalhossaini, Carcinoembryonic antigen expression level as a predictive factor for response to 5-fluorouracil in colorectal cancer, Mol. Biol. Rep. 41 (1) (2014) 459–466.
[18] Bijuli Rabha, Kaushik Kumar Bharadwaj, Siddhartha Pati, Bhabesh Kumar Choudhury, Tanmay Sarkar, Zulhisyam Abdul Kari, Hisham Atan Edinur, Debabrat Baishya, Leonard Ionut Atanase, Development of polymer-based nanoformulations for glioblastoma brain cancer therapy and diagnosis: an update, Polymers 13 (23) (2021) 4114.
[19] B. Zhang, Y. Wang, G. Zhai, Biomedical applications of the graphene-based materials, Mater. Sci. Eng. C Mater. Biol. Appl. 61 (2016) 953–964.
[20] W.S. Hummers Jr, R.E. Offeman, Preparation of graphitic oxide, J. Am. Chem. Soc. 80 (1958) 1339, 1339.
[21] H. Shen, L. Zhang, M. Liu, Z. Zhang, Biomedical applications of graphene, Theranostics 2 (2012) 283–294.
[22] Wenjun Feng, Zhengke Wang, Biomedical applications of chitosan-graphene oxide nanocomposites, iScience (2021), 103629.
[23] Bo Xue, Yuehua Wang, Jinlong Tian, Weijia Zhang, Zhihuan Zang, Huijun Cui, Ye Zhang, Qiao Jiang, Bin Li, Rui Hai Liu, Effects of chitooligosaccharide-functionalized graphene oxide on stability, simulated digestion, and antioxidant activity of blueberry anthocyanins, Food Chem. 368 (2022), 130684.
[24] Sunil Kumar Dubey, Tanya Bhatt, Mukta Agrawal, Ranendra Narayan Saha, Swarnlata Saraf, Shailendra Saraf, Alexander Amit, Application of chitosan modified nanocarriers in breast cancer, Int. J. Biol. Macromol. 194 (2022) 521–538.
[25] J.R. Cardinal, W.J. Curatolo, C.D. Ebert, Chitosan Compositions for Controlled and Prolonged Release of Macromolecules, 1990.

[26] Amirmasoud Samadi, et al., Curcumin-loaded chitosan-agarose-montmorillonite hydrogel nanocomposite for the treatment of breast cancer, in: 2020 27th National and 5th International Iranian Conference on Biomedical Engineering (ICBME), IEEE, 2020.
[27] Zavareh, Hediyeh Sepahi, et al., Chitosan/carbon quantum dot/aptamer complex as a potential anticancer drug delivery system towards the release of 5-fluorouracil, Int. J. Biol. Macromol. 165 (2020) 1422–1430.
[28] Z.C. Yin, Y.L. Wang, K. Wang, A pH-responsive composite hydrogel beads based on agar and alginate for oral drug delivery, J. Drug Deliv. Sci. Technol. 43 (2018) 12–18.
[29] Chulgu Kim, et al., Cyclodextrin functionalized agarose gel with low gelling temperature for controlled drug delivery systems, Carbohydr. Polym. 222 (2019), 115011.
[30] C.M. Daniela, V.K. Dmitry, M.B. Jacob, S. Alexander, S. Zhengzong, S. Alexander, B.A. Lawrence, L. Wei, M.T. James, Improved synthesis of graphene oxide, ACS Nano 4 (2010) 4806–4814.
[31] S. Jahanizadeh, F. Yazdian, A. Marjani, M. Omidi, H. Rashedi, Curcumin-loaded chitosan/carboxymethyl starch/montmorillonite bionanocomposite for reduction of dental bacterial biofilm formation, Int. J. Biol. Macromol. 105 (2017) 757–763.
[32] Bakht Ramin Shah, et al., Preparation and optimization of Pickering emulsion stabilized by chitosan-tripolyphosphate nanoparticles for curcumin encapsulation, Food Hydrocolloids 52 (2016) 369–377.
[33] C. Nanocomposites, M. Abbasian, F. Mahmoodzadeh, A. Khalili, R. Salehi, Chemotherapy of breast cancer cells using novel pH-responsive, Tabriz Univ. Med. Sci. 9 (2019) 122–131.
[34] M. Kakran, N.G. Sahoo, L. Li, Dissolution enhancement of quercetin through nanofabrication, complexation, and solid dispersion, Colloids Surf. B Biointerfaces 88 (2011) 121–130.
[35] S. Jeon, C.Y. Yoo, S.N. Park, Improved stability and skin permeability of sodium hyaluronate-chitosan multilayered liposomes by Layer-by-Layer electrostatic deposition for quercetin delivery, Colloids Surf. B Biointerfaces 129 (2015) 7–14.
[36] R.F. Melo-Silveira, G.P. Fidelis, M.S.S. Pereira Costa, C.B.S. Telles, N. Dantas-Santos, S. de Oliveira Elias, V.B. Ribeiro, A.L. Barth, A.J. Macedo, E.L. Leite, H.A. O. Rocha, In vitro antioxidant, anticoagulant and antimicrobial activity and in inhibition of cancer cell proliferation by xylan extracted from corn cobs, Int. J. Mol. Sci. 13 (2012) 409–426.
[37] W.F. Wolkers, A.E. Oliver, F. Tablin, J.H. Crowe, A Fourier-transform infrared spectroscopy study of sugar glasses, Carbohydr. Res. 339 (2004) 1077–1085.
[38] F.R.F. Silva, C.M.P.G. Dore, C.T. Marques, M.S. Nascimento, N.M.B. Benevides, H. A.O. Rocha, S.F. Chavante, E.L. Leite, Anticoagulant activity, paw edema and pleurisy induced carrageenan: action of major types of commercial carrageenans, Carbohydr. Polym. 79 (2010) 26–33.
[39] S.H. Lim, S.M. Hudson, Synthesis and antimicrobial activity of a water-soluble chitosan derivative with a fiber-reactive group, Carbohydr. Res. 339 (2004) 313–319.
[40] M.F. Queiroz, K.R.T. Melo, D.A. Sabry, G.L. Sassaki, H.A.O. Rocha, Does the use of chitosan contribute to oxalate kidney stone formation? Mar. Drugs 13 (2015) 141–158.
[41] D. Han, L. Yan, W. Chen, W. Li, Preparation of chitosan/graphene oxide composite film with enhanced mechanical strength in the wet state, Carbohydr. Polym. 83 (2011) 653–658.
[42] Z. Zarei, B. Akhlaghinia, Cu(II) immobilized on Fe3O4@Agarose nanomagnetic catalyst functionalized with ethanolamine phosphate– salicylaldehyde schiff base: a magnetically reusable nanocatalyst for preparation of 2-substituted imidazolines, oxazolines, and thiazolines, Turk. J. Chem. 42 (2018) 170–191.
[43] Jianguo Song, Xinzhi Wang, Chang-Tang Chang, Preparation and characterization of graphene oxide, J. Nanomater. (2014) 2014.
[44] X. Sun, Z. Liu, K. Welsher, J.T. Robinson, A. Goodwin, S. Zaric, H. Dai, Nano-graphene oxide for cellular imaging and drug delivery, Nano Res. 1 (3) (2008) 203–212.
[45] P.R. Sivashankari, M. Prabaharan, Three-dimensional porous scaffolds based on agarose/chitosan/graphene oxide composite for tissue engineering, Int. J. Biol. Macromol. 146 (2020) 222–231.
[46] X.H. Li, J. Feng, Y.P. Du, J.T. Bai, H.M. Fan, H.L. Zhang, et al., One-pot synthesis of $CoFe_2O_4$/graphene oxide hybrids and their conversion into FeCo/graphene hybrids for lightweight and highly efficient microwave absorber, J. Mater. Chem. 3 (10) (2015) 5535–5546.
[47] Hamid Rahmani, Fattahi Ali, Komail Sadrjavadi, Salar KhalediaI, Yalda Shokoohinia, Preparation and characterization of silk fibroin nanoparticles as a potential drug delivery system for 5-fluorouracil, Adv. Pharmaceut. Bull. 9 (4) (2019) 601–608.
[48] R.L. Siegel, K.D. Miller, A. Jemal, Cancer statistics,CA, A Cancer Journal for clinicians 66 (1) (2016) 7–30.
[49] Malihe Pooresmaeil, Elnaz Aghazadeh Asl, Namazi Hassan, A new pH-sensitive CS/Zn-MOF@ GO ternary hybrid compound as a biofriendly and implantable platform for prolonged 5-Fluorouracil delivery to human breast cancer cells, J. Alloys Compd. 885 (2021), 160992.
[50] Dongliang Shi, et al., Design and synthesis of chitosan/agar/Ag NPs: a potent and green bio-nanocomposite for the treatment of glucocorticoid induced osteoporosis in rats, Arab. J. Chem. 15 (1) (2022), 103471.
[51] J.A. Luceño-Sánchez, A. Charas, A.M. Díez-Pascual, Effect of HDI-modified GO on the thermoelectric performance of poly(3,4-ethylenedioxythiophene):poly (styrenesulfonate) nanocomposite films, Polymers 13 (2021) 1503.
[52] Puwang Li, Ziming Yang, Yichao Wang, Peng Zheng, Sidong Li, Lingxue Kong, Qinghuang Wang, Microencapsulation of coupled folate and chitosan nanoparticles for targeted delivery of combination drugs to colon, J. Microencapsul. 32 (1) (2015) 40–45.
[53] R.A. Praphakar, M. Jeyaraj, S. Mehnath, A. Higuchi, Dalekshmi Ponnamma, K. Kumar Sadasivunid, M. Rajan, A pH-sensitive guar gum-grafted-lysine-bcyclodextrin drug carrier for the controlled release of 5-flourouracil into cancer cells, J. Mater. Chem. B 6 (2018) 1519.
[54] G. Prabha, V. Raj, Preparation and characterization of chitosan - polyethylene glycol -polyvinylpyrrolidone-coated superparamagnetic iron oxide nanoparticles as carrier system: drug loading and in vitro drug release study, J. Biomed. Mater. Res. Part B Appl. Biomater. 104 (2016) 808–816.
[55] A. Sedaghat Doost, V. Kassozi, C. Grootaert, M. Claeys, K. Dewettinck, J. Van Camp, P. Van der Meeren, Self-assembly, functionality, and in-vitro properties of quercetin loaded nanoparticles based on shellac-almond gum biological macromolecules, Int. J. Biol. Macromol. 129 (2019) 1024–1033.
[56] M. Mahdi Eshaghi, M. Pourmadadi, A. Rahdar, A.M. Díez-Pascual, Novel carboxymethyl cellulose-based hydrogel with core–shell Fe3O4@SiO2 nanoparticles for quercetin delivery, Materials 15 (2022) 8711.
[57] Irfa Basharat Rajput, Fahad Khan Tareen, Atif Ullah Khan, Naveed Ahmed, Muhammad Farhan Ali Khan, Kifayat Ullah Shah, Abbas Rahdar, M. Ana, Díez Pascual, Fabrication and in vitro evaluation of chitosan-gelatin based aceclofenac loaded scaffold, Int. J. Biological. Macomol. 224 (2023) 223–232.
[58] H. Jin, X. Liu, R. Gui, Z. Wang, Facile synthesis of gold nanorods/hydrogels core/shell nanospheres for pH and near-infrared-light induced release of 5-fluorouracil and chemo-photothermal therapy, Colloids Surf. B Biointerfaces 128 (2015) 498–505.
[59] T. Moodley, M. Singh, Polymeric mesoporous silica nanoparticles for enhanced delivery of 5-fluorouracil in vitro, Pharmaceutics 11 (2019) 288.
[60] E. Nivethaa, S. Dhanavel, V. Narayanan, C.A. Vasu, A. Stephen, An in vitro cytotoxicity study of 5-fluorouracil encapsulated chitosan/gold nanocomposites towards MCF-7 cells, RSC Adv. 5 (2015) 1024–1032.
[61] P. Li, Y. Wang, Z. Peng, F. She, L. Kong, Development of chitosan nanoparticles as drug delivery systems for 5-fluorouracil and leucovorin blends, Carbohydr. Polym. 85 (2011) 698–704.
[62] S. Amirmasoud, M. Pourmadadi, F. Yazdian, H. Rashedi, Mona Navaei-Nigjeh, Ameliorating quercetin constraints in cancer therapy with pH-responsive agarose-polyvinylpyrrolidone-hydroxyapatite nanocomposite encapsulated in double nanoemulsion, Int. J. Biol. Macromol. 182 (2021) 11–25.
[63] Alexandra ML. Oliveira, Mónica Machado, Gabriela A. Silva, Diogo B. Bitoque, Joana Tavares Ferreira, Luís Abegão Pinto, Quirina Ferreira, Graphene oxide thin films with drug delivery function, Nanomaterials 12 (7) (2022) 1149.
[64] N.T. Si, P.V. Nhat, M.T. Nguyen, Binding mechanism and SERS spectra of 5-fluorouracil on gold clusters, Front. Chem. 10 (2022), 1050423.